Geometrical perturbation of graphene electronic structure

Paul E. Lammert and Vincent H. Crespi
Department of Physics and Center for Materials Physics, The Pennsylvania State University, 104 Davey Lab, University Park, Pennsylvania 16802-6300

(Received 2 July 1999; revised manuscript received 13 October 1999)

We discuss low-energy electronic properties of distorted graphene sheets from a local geometric viewpoint, treating curvature and strain as perturbations of a smooth surface. This allows a unified description of the variety of deformations to which carbon nanotubes are susceptible. By using a general symmetry analysis in conjunction with a four-orbital, nonorthogonal tight-binding model, we calculate accurate values of the relevant couplings.

Carbon nanotubes[1] have a high Young's modulus, but are not otherwise mechanically strong, being easily bent, or deformed by van der Waals interactions with a substrate.[2] Hence, the electronic repercussions of mechanical deformations are of interest for both fundamental and device-oriented reasons. Kane and Mele[3] have studied this issue with the aid of a tight-binding model incorporating only π electrons. We use a model-independent group-theoretical analysis to reveal the relevant couplings, which are then evaluated with a four-orbital non-orthogonal tight-binding model that takes into account the strong effects of rehybridization. By expressing curvature and strain as a modification of the Hamiltonian and overlap, we avoid the use of the large unit cells implied by small deformations.

The response of electronic structure to curvature and strain is essentially a local coupling, largely independent of boundary conditions or global topology. We therefore isolate the effects of geometric deformation by first studying a single graphene sheet. Although our perturbative approach is in principle limited to gentle distortions, the results are in good agreement with full tight-binding calculations for a radius of curvature as small as two graphene lattice spacings [i.e., a (12,0) tube].

The conformation of a surface in space (e.g., a single graphene sheet) is described by a vector-valued embedding function $\mathbf{X}(x^\mu)$, specifying the location of the point with coordinates $x^\mu, \mu=1,2$. The pair of vectors $\boldsymbol{\tau}_\mu = \partial\mathbf{X}/\partial x^\mu, (\mu = 1,2)$ provide a basis for the tangent space and determine the metric $g_{\mu\nu} = \boldsymbol{\tau}_\mu \cdot \boldsymbol{\tau}_\nu$, which converts coordinate differences into physical distances. If the coordinates are determined relative to a flat unstretched state, the metric carries information about strain. The inverse of this matrix is denoted $g^{\lambda\sigma}$, so that $g^{\lambda\mu} g_{\mu\nu} = \delta^\lambda{}_\nu$. Curvature is detected by second derivatives[4,5] of the embedding function $\mathbf{X}$,

$$\frac{\partial \boldsymbol{\tau}_\nu}{\partial x^\mu} = \hat{\mathbf{n}} K_{\nu\mu} + \boldsymbol{\tau}_\lambda \Gamma^\lambda{}_{\nu\mu}, \tag{1}$$

where $\hat{\mathbf{n}}$ is the unit vector normal to the surface, the sign of which is chosen arbitrarily. The extrinsic curvature $K_{\mu\nu}$ describes the way the surface is embedded in space, and the connection coefficients $\Gamma^\lambda{}_{\mu\nu}$ are mostly related to twisting of the coordinates from point to point on the surface. A similar equation

$$\frac{\partial \hat{\mathbf{n}}}{\partial x^\mu} = -\boldsymbol{\tau}_\nu K^\nu{}_\mu \tag{2}$$

obtains for the derivatives of the unit normal vector. An index was raised here with the metric as usual: $K^\mu{}_\nu = g^{\mu\lambda} K_{\lambda\nu}$. At each point, a surface has two principal curvatures $1/R_1$ and $1/R_2$ along orthogonal directions. The Gaussian curvature, $G = 1/(R_1 R_2)$, is related to the extrinsic curvature by

$$G = \det K^\mu{}_\nu, \tag{3}$$

where the indices indicate which version of K to use.

Figure 1 depicts the graphene lattice and its first Brillouin zone. Bands cross the Fermi level only at the isolated points K and K' at the corners of the zone. We exploit their stabilizer (little) group to constrain the form of an effective Hamiltonian for the electronic states near the Fermi energy. The full point group of the graphene lattice is D_{6h}, which is generated by a rotation through $\pi/3$ about an axis ($\hat{\mathbf{z}}$) perpendicular to the plane, reflection through the x-y plane (σ_h), and rotations by π about axes through lattice points or halfway between, as depicted in Fig. 1(b). K is not invariant under rotations by odd multiples of $\pi/3$, so its stabilizer sub-

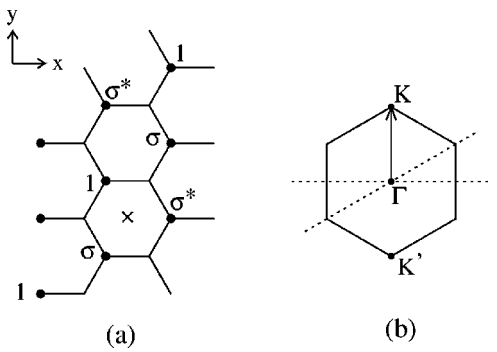

FIG. 1. (a) The pattern of phases associated with the Brillouin zone point K, which we take to point along the y direction; all sites at the same value of y have the same phase and we abbreviate $\sigma = e^{2\pi i/3}$. The sites with heavy dots are on the A sublattice. (b) The points K and K' in the hexagonal Brillouin zone, and the two types of π rotation axes in the stabilizer group of K.

 ©2000 The American Physical Society

group is D_{3h}. We focus on an Abelian subgroup, C_{3h}, generated by the $2\pi/3$ rotation about $\hat{\mathbf{z}}$ and the mirror plane.

Transformation of tensors such as $g_{\mu\nu}$ and $K_{\mu\nu}$ is facilitated by use of the complex coordinates

$$z=\frac{1}{\sqrt{2}}(x+iy), \quad \bar{z}=\frac{1}{\sqrt{2}}(x-iy). \tag{4}$$

In these coordinates, the Euclidean metric has components

$$\begin{pmatrix} g_{zz} & g_{z\bar{z}} \\ g_{\bar{z}z} & g_{\bar{z}\bar{z}} \end{pmatrix}=\begin{pmatrix} 0 & 1 \\ 1 & 0 \end{pmatrix}. \tag{5}$$

The inverse $g^{\mu\nu}$ is the same matrix as $g_{\mu\nu}$, so that raising or lowering an index does not change the numerical value of a tensor component. The general relation between the $z,\bar{z}$ and the ordinary Cartesian components of a second-rank tensor is

$$A_{zz}=\tfrac{1}{2}[A_{xx}-A_{yy}-i(A_{xy}+A_{yx})],$$

$$A_{z\bar{z}}=\tfrac{1}{2}[A_{xx}+A_{yy}+i(A_{xy}-A_{yx})].$$

$A_{\bar{z}\bar{z}}$ and $A_{\bar{z}z}$ are obtained by complex conjugation. If A is symmetric (as are g and K) $A_{z\bar{z}}$ is real.

For a given tensor component $A^{\cdots}{}_{\cdots}$, we define an integer ''spin,'' s = # (upper z's and lower $\bar{z}$'s) − # (lower z's and upper $\bar{z}$'s). If the geometrical structure described by a uniform value of the tensor A is rotated counterclockwise through an arbitrary angle θ, each component picks up a phase factor of $e^{is\theta}$.

The electronic states at K decompose into one-dimensional representations of C_{3h} labeled again by a spin, so that under rotation by $2\pi/3$ counterclockwise about a hexagon center, a state picks up a phase factor of $e^{i2\pi s/3}$. At the Fermi level there are two states, one (A) having the pattern of amplitudes depicted in Fig. 1(a), and another (B) which differs only in having that pattern shifted perpendicular to K onto the B sublattice. They have the following attributes, where $\chi(\sigma_h)$ indicates evenness $(+1)$ or oddness (-1) under reflection through the graphene plane:

$$A: \quad s=-1, \quad \chi(\sigma_h)=-1,$$

$$B: \quad s=+1, \quad \chi(\sigma_h)=-1.$$

The corresponding states at K' have spins with opposite sign.

The effective Hamiltonian contains only terms that are even under σ_h and have total spin zero (mod 3). The kinetic part associated with the undeformed sheet is

$$H_{\mathrm{D}}(q)=\sqrt{2}v_{\mathrm{F}}\begin{pmatrix} 0 & -iq^{z} \\ iq^{\bar{z}} & 0 \end{pmatrix}, \tag{6}$$

where the upper row (left column) corresponds to A, and the lower row (right column) to B. Here and below, we omit creation and destruction operators.

The curvature and strain-induced effective potential (in the sense of a self-energy) for these two bands takes the form

$$V=\begin{pmatrix} V_{AA} & V_{AB} \\ V_{BA} & V_{BB} \end{pmatrix}, \tag{7}$$

the components of which are restricted by symmetry as follows. All elements are even under the mirror operation σ_h. $V_{AB}=(V_{BA})^*$ has spin 1 (mod 3). V_{AA} and V_{BB} must be real, simply from self-adjointness. Finally, using σ_v, V_{BB} is found from V_{AA} by changing the sign of terms with odd tensor order.

The only allowed combinations to lowest nontrivial order in $\delta g_{\mu\nu}$ and $K_{\mu\nu}$ (first and second, respectively) are straightforward to determine. The spins of the metric and curvature are clear from the indices they carry. Under σ_h, δg is even, but $K_{\mu\nu}$ is odd because of its dependence on the choice of orientation of the unit normal **n**. The connection coefficients can be ignored because they are second order in gradients of the metric, and all the information they contain about curvature is already found in $\det K$. This analysis produces an effective potential

$$V_{AA}=c_1\,\mathrm{Tr}\,\delta g+c_2(\mathrm{Tr}\,K/2)^2+c_3G,$$

$$V_{BB}=V_{AA}, \tag{8}$$

$$V_{AB}=c_4\delta g_{zz}+c_5(K_{z\bar{z}})^2+c_6K_{zz}K_{z\bar{z}}.$$

$\mathrm{Tr}\,K/2=K_{z\bar{z}}$ is the mean curvature, and $G=|K_{zz}|^2-|K_{z\bar{z}}|^2$ is the Gaussian curvature.

To compute the values of the couplings, we employ a four orbital per atom, nonorthogonal tight-binding model, with the parametrizations of Porezag *et al.*[10] Curvature induces nonzero Hamiltonian and curvature matrix elements between local π orbitals and sp^2 orbitals. Although the result can be recast as a π Hamiltonian (as for instance in Ref. 3), accurate computation of the effect requires all the orbitals since bending produces rehybridization.

We choose a basis of p orbitals on each atom to correspond to an orthonormal frame having the third element normal to the surface. The Hamiltonian then connects orbitals on different sites according to a 4×4 matrix depending upon the distance between them as well as the relative orientation of the frames. The curvature enters both of these quantities, since it affects the relation between coordinate differences (along the sheet) and the interatomic distance. Neglecting the change in interatomic distance results in calculated gaps reduced by a factor of 2.

We extract the couplings $c_1,\ldots,c_6$ from the four-orbital tight-binding model by studying the motion of the Fermi point under very small deformations of a graphene sheet. The error incurred by truncating the expansion as in Eq. (8) can be gauged from Fig. 2. The departure from the lowest-order curvature-induced effects does not exceed 10% up to the equivalent of a (6,6) tube. Similarly, the strain dependence is nearly linear up to 10% extension.

The curvature affects orientations and positions of the relevant atomic orbitals. By shifting this dependence onto the Hamiltonian and overlap matrices, we make the problem appear as a flat sheet with unorthodox couplings. This is somewhat analogous to the shift from Schrödinger to Heisenberg representations. Under uniform curvature conditions, this restores a two-atom unit cell so that computations are rapid and individual couplings easily isolated. The computed values of the c_n are collected in Table I.

The symmetry under $y\to-y$ guarantees that all the c_i are real. Comparison with the kinetic Hamiltonian [Eq. (6)]

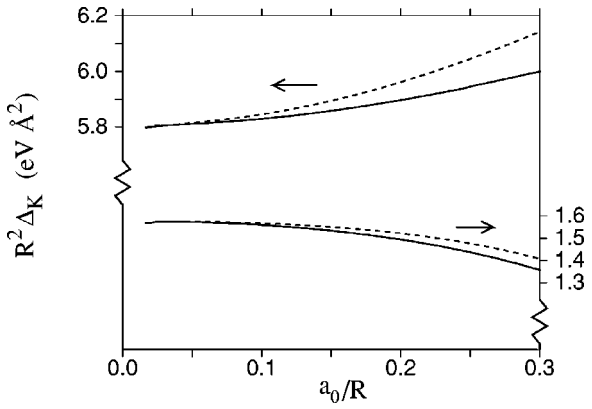

FIG. 2. Curvature induces an energy difference Δ_K between the two bands at K by shifting the Fermi point. This results in a genuine energy gap if the shifted point is not accessible due to boundary conditions. Δ_K is shown scaled by R^2 here for $\chi=0$ (upper curves, left-hand scale) and $\chi=\pi/6$ (lower curves, right-hand scale). Note the zero offset. ($a_0=2.46$ Å is the graphene lattice constant.) The solid curves are exact. Expanding the Hamiltonian and overlap only to quadratic order in $K_{\mu\nu}$ results in the dashed curves.

shows that distorting the sheet shifts the double cone of the low-energy bands in both **q** and energy. However, it is of interest to note that the Fermi point is never destroyed to this order and persists in the infinite graphene sheet. A gap can be induced only if boundary conditions make the shifted Fermi point inaccessible, as occurs in a cylindrical geometry. As for the strain contributions, Tr $\delta g = g_{xx}+g_{yy}=2\,\delta g_{z\bar{z}}$ measures isotropic dilatation or compression of the lattice. The other component, $g^{z}{}_{\bar{z}}=\frac{1}{2}(g_{xx}-g_{yy}+2ig_{xy})$, is associated with shear (twisting, for a tube). Since **k** vectors are reckoned with respect to coordinates attached to the undeformed conformation, a dilatation does not shift the Fermi point at all. Also note that the gradient of the curvature $K_{\mu\nu}$ cannot contribute to V even in higher order, because it is odd under σ_h.

Cylindrical geometries and perturbations of them are of special interest. We use a right-handed system of ''tube coordinates'' ξ and ζ with $\hat{\boldsymbol{\xi}}$ running along the circumference and $\hat{\boldsymbol{\zeta}}$ along the axial direction of the cylinder (so that $\hat{\boldsymbol{\xi}}\times\hat{\boldsymbol{\zeta}}$ points outward[3]). These combine into $w=(\xi+i\zeta)/\sqrt{2}$ and its complex conjugate $\bar{w}$. Introducing the wrapping angle χ between the circumferential direction ξ and a bond direction x, we have $w=e^{-i\chi}z$. Similarly, $q^w=(q_\xi+iq_\zeta)/\sqrt{2}=e^{-i\chi}q^z$. The values of q_ξ are quantized to $2\pi n/R$, where R is the cylinder radius. With this substitution, the kinetic Hamiltonian becomes

TABLE I. Geometric couplings in graphene.

Coupling	Value ($a_0=2.46$ Å)
c_1	-1.06 ± 0.05 eV
c_2	1.324 ± 0.005 eV a_0^2
c_3	-0.900 ± 0.005 eV a_0^2
c_4	7.00 ± 0.05 eV
c_5	-0.699 ± 0.002 eV a_0^2
c_6	-1.221 ± 0.003 eV a_0^2

$$H_{\mathrm{D}}(q)=i\sqrt{2}v_{\mathrm{F}}\begin{pmatrix}0 & -e^{i\chi}q^{w}\\ e^{-i\chi}q^{\bar{w}} & 0\end{pmatrix}.$$

It is well known[6] that curvature can induce a gap in a nanotube. We now demonstrate how this effect arises from the geometrical couplings. If the cylinder is undistorted, $K_{ww}=K_{w\bar{w}}=1/2R$. The $z,\bar{z}$ components have this same magnitude, but different phases according to their spins, so that the off-diagonal element of the effective potential becomes

$$V_{AB}^{\mathrm{cyl}}=\frac{e^{i\chi}}{4R^2}(c_5e^{3i\chi}+c_6e^{-3i\chi})+c_4e^{-2i\chi}\delta g_{ww}, \qquad (9)$$

where anisotropic strain in the bonds is accounted for by δg. The imaginary part of the factor in parentheses can be offset by a shift of q_ζ, but the real part cannot, and q_ξ is quantized. The curvature therefore induces a direct gap of magnitude

$$\Delta_0=\left|\frac{c_5-c_6}{2R^2}\sin 3\chi\right|, \qquad (10)$$

which is shifted away from K by $q_\zeta^0=-[(c_5+c_6)/4R^2]\cos 3\chi$. The value of the constant $|c_5-c_6|/2$ is about 0.26 eV a_0^2 (see Table I). Notice that (n,n) tubes are not gapped by curvature or by δg, since δg_{ww} is real for these achiral tubes.

Now we consider deformations imposed on the uniform cylindrical background curvature. Since circumferential boundary conditions reduce each band for planar graphene to a set of separated branches, we construct an effective potential for the lowest-lying branch only. (n,n) tubes ($\chi=0$) are of most interest, since they remain ungapped in the uniform conformation.

In a left/right-moving basis which diagonalizes the kinetic energy,

$$H=\begin{pmatrix}-v_{\mathrm{F}}q_\zeta+\mathrm{Re}\,V_{AB}+V_{AA} & -i\,\mathrm{Im}\,V_{AB}\\ i\,\mathrm{Im}\,V_{AB} & v_{\mathrm{F}}q_\zeta-\mathrm{Re}\,V_{AB}+V_{AA}\end{pmatrix}. \qquad (11)$$

Circumferential averaging is implicit here and the zero of q_ζ has been shifted.

In general, the diagonal part of V shifts the Fermi point in q_ζ and the entire band structure in energy. Such a shift is relevant to an intratube junction, which could be created by, e.g., local squashing of a tube. This involves additional direct electronic coupling as well as curvature effects as has been discussed elsewhere.[7] Meanwhile, the off-diagonal term can open a gap or scatter electrons between left- and right-moving branches.

The application of our effective Hamiltonian to the electronic effects of mechanical deformations, either externally imposed or thermally excited, requires consideration of the elastic properties of a nanotube. The lowest-energy deformations of the tube are the bending and twisting[3,9] Goldstone modes. In comparison to strain, curvature costs very little elastic energy. For instance, a (10,10) tube has an E_{2g} 'squashing' mode[8] at 3 meV and a breathing mode at 20 meV. To study the low-energy modes, we parametrize the deformation by local changes in radius, $h(\xi,\zeta)$, and azimuth,

$\theta(\xi,\zeta)$. Strain energy is approximately minimized by discarding azimuthally uniform changes in radius, and setting $\partial_\xi\theta + h = 0$. Only the azimuthally uniform part θ_0 of θ and nonuniform Fourier modes of h are independent variables. We also discard higher than first derivatives in ζ. The result, after azimuthal averaging, is

$$\mathrm{Im}\, V_{AB} \approx \left[\frac{1}{R^2}\left(\frac{c_6}{2}-c_5\right)-c_4\right] R\partial_\zeta\theta_0 + \left(\frac{c_6}{2}-c_5\right)\partial_\xi^2 h(\partial_\xi\partial_\zeta h) - c_4(\partial_\xi h)(\partial_\zeta h).$$

Since the strain coupling c_4 is about 7 eV and the combination $c_5 - c_6/2$ of curvature couplings is about 0.1 eV a_0^2, pure curvature couples very weakly. Moreover, in the approximation we have made, there is absolutely no coupling without axial variation of the deformation, and that necessarily implies strain, so that the major part of any elastic normal mode will couple primarily through strain.

This geometric picture provides a unified framework for understanding the effects of structural distortions, both curvature and strain, on the low-energy electronic properties of sp^2-bonded carbon, particularly nanoscale materials such as nanotubes and nanocones.[11] The effective Hamiltonian so produced can handle large-scale distortions in a natural and computationally efficient manner, using a minimal (two-atom) unit cell.

We gratefully acknowledge the David and Lucile Packard Foundation and the Research Corporation; and the support of the National Science Foundation through Grant No. DMR-9876232, and the Petroleum Research Fund of the American Chemical Society through Grant No. 73824-65. We also thank Eduardo Hernandez for providing the tight-binding parameters and assistance in developing the band structure code.

[1] S. Iijima, Nature (London) **354**, 56 (1991).
[2] T. Hertel, R.E. Walkup, and Ph. Avouris, Phys. Rev. B **58**, 13 870 (1998).
[3] C.L. Kane and E.J. Mele, Phys. Rev. Lett. **78**, 1932 (1997).
[4] W.M. Boothby, *An Introduction to Differentiable Manifolds and Riemannian Geometry*, 2nd ed. (Academic Press, Orlando, 1986).
[5] M. Spivak, *A Comprehensive Introduction to Differential Geometry*, Vol. 2 (Publish or Perish, Houston, 1979).
[6] N. Hamada, S. Sawada, and A. Oshiyama, Phys. Rev. Lett. **68**, 1579 (1992).
[7] P.E. Lammert, P. Zhang, and V.H. Crespi (unpublished).
[8] A.M. Rao *et al.*, Science **275**, 187 (1997). The frequency of the squashing mode is proportional to $1/R^2$, that of the breather to $1/R$.
[9] C.L. Kane, E.J. Mele, R.S. Lee, J.E. Fischer, P. Petit, H. Dai, A. Thess, R.E. Smalley, A.R.M. Vershueren, S.J. Tans, and C. Dekker, Europhys. Lett. **41**, 683 (1998).
[10] D. Porezag, Th. Frauenheim, Th. Köhler, G. Seifert, and R. Kaschner, Phys. Rev. B **51**, 12 947 (1995).
[11] A. Krishnan, E. Dujardin, M.M.J. Treacy, J. Hugdahl, S. Lynum, and T.W. Ebbesen, Nature (London) **388**, 451 (1997).